CFD Investigation for Surface Roughness Effects on the Hydrodynamics of Cavitating Turbulent Flow through a Low Head Prototype Francis Turbine

G. Tiwari[1†], J. Kumar[1], V. Prasad[2] and V. K. Patel[1]

[1] Applied Mechanics Department, MNNIT Allahabad, Prayagraj, Uttar Pradesh, 211004, India
[2] Department of Civil Engineering, MANIT, Bhopal, Madhya Pradesh, 462003, India

†*Corresponding Author Email: ram1602@mnnit.ac.in*

ABSTRACT

Surface characteristics have an important role in defining hydrodynamics of the flow through hydraulic machines. Surface roughness is a critical parameter that contributes to altering near-wall flow features and promotes frictional losses in various components of a water turbine. The nature of flow through the Francis turbine runner is highly complex, especially at cavitating regimes, and the surface roughness effects add to the flow complexity. The present work is aimed at evaluating surface roughness effects on the cavitation performance of a low head prototype Francis turbine computationally. Complete cavitation characteristic of the turbine is derived with the consideration of smooth and rough boundaries by implementing SST k-ω turbulence model and cavitation model based on the Rayleigh-Plesset equation, and a comparative study is carried out comprehensively. For the analysis, the complete flow domain of the turbine is considered, and the simulations are conducted for four different operating conditions from the part load of 60% to overload of 120%. Different values of equivalent sand grain roughness, ks, are assigned to different components of the turbine by following the International Electro-Technical Commission standard IEC 62097 Edition-2. It is concluded that the surface roughness effects on the performance of the turbine in the absence of cavitation are not significant for operation at BEP but for the part load of 60% and overload operations, it has considerable hydrodynamic effects. However, these effects become more detrimental at developed cavitation regimes. The obtained computational results are found in a fair agreement with the available experimental results and are quite consistent with the previous research.

Keywords: Flow hydrodynamics; Surface roughness; Cavitation; Francis turbine; CFD.

NOMENCLATURE

k_s	equivalent sand grain roughness height	R_B	bubble radius
m_{fg}	total mass transfer rate at the interface	S_E	energy source
P	pressure	S_M	momentum source
P_v	pressure in the bubble/ vapour pressure at the working temperature	ρ	density of the fluid
		ρ_f	liquid density
r_{nuc}	nucleation site volume fraction	σ	surface tension coefficient at water-vapour interface
R_a	arithmetic average roughness height		
R_{nuc}	nucleation radius	τ_{ij}	viscous stress tensor

1. INTRODUCTION

The fastest-growing demand for power persuades engineers to develop highly efficient and economically feasible power systems like hydropower (Tiwari *et al.* 2020a). Moreover, hydropower as green energy is very promising (Ayancik *et al.* 2017) among other renewable energy sources (Khare *et al.* 2020) due to its high agility of switching operating regimes according to the load demand and continuous power generation capabilities (Tiwari *et al.* 2020b,c). The development of hydropower systems needs highly sophisticated modern water turbines (Tiwari *et al.*, 2020a) having higher specific speeds which result in less weight and dimensions of turbine components. Consequently,

smaller turbine and generator sizes (Barlit, 2007) are indeed economical. But, going for higher specific speeds leads to higher flow velocities and associated energy loss in different components of the turbine (Tiwari *et al.* 2020d). This is a condition of dynamic vacuum wherein absolute pressure decreases sharply (Celebioglu *et al.* 2017). If the absolute pressure at any location of the turbine decreases to a value equal to or less than vapour pressure of the water at the working temperature, the phenomenon cavitation occurs. Improper design and off-design regimes of operation can cause cavitation in hydraulic turbines (Lahdelma and Juuso 2008). It deteriorates the performance of the turbine and can damage its space. Damage caused by cavitation may lead to several weeks of operation delay (Luo *et al.* 2016). Performances of hydraulic turbines show a clear declination after a few years of operation due to cavitation as it causes flow instabilities, noise, and vibration resulting from surface damage (Escaler *et al.* 2006). Cavitation in hydraulic turbines can occur in different ways depending on the design and regimes of operation (Zhang and Zhang 2012). It cannot be avoided completely, but its strength can be minimized to an economically acceptable level.

The Cavitation is a three-dimensional, discontinuous, and unsteady phenomenon that is very difficult to capture accurately through any approach (Barlit 2007; Gohil and Saini 2016). CFD plays an important role (Drtina and Sallaberger 1999) in analyzing the cavitating flows and provides a detailed inspection that suggests necessary measures for improving turbine cavitation characteristics by the modification of turbine space and runner blades shape (Kumar and Saini 2010). Also, Reynolds averaged Navier-Stokes (RANS) based CFD simulations are high fidelity solutions to governing equations including viscous effects (Dutta *et al.* 2016; Laouari and Ghenaiet 2016; Liu *et al.* 2009; Tiwari *et al.* 2020e). Moreover, analysis of cavitation using CFD is a cost-effective solution (Kumar *et al.* 2020a, b; Luo *et al.* 2016; Zuo *et al.* 2015). Researchers performed many experimental and numerical analyses to develop a better understanding of cavitation in hydraulic turbines (Celebioglu *et al.* 2017).

During the fabrication of a hydraulic turbine, one of the major concerns is the surface finish of different turbine components as inappropriate roughness size may lead to excessive hydraulic energy loss and uneconomical turbine operation. The frictional loss due to surface roughness is one of the important issues which results in performance degradation (Gohil and Saini 2014) and needs to be addressed in order to understand the hydrodynamic phenomena associated with the surface roughness. Maruzewski *et al.* (2009) carried out a computational work for predicting specific energy loss in each component of a Francis turbine with the consideration of rough boundaries by specifying different sand grain roughness values to each component. It was concluded that local friction loss can be accurately predicted through CFD approach while simulating flow over rough boundaries. However, certain studies showed that surface roughness can contribute

to small efficiency gains under specific flow conditions. The surface roughness of runner blades may assist in a little gain in hydraulic efficiency due to delayed flow separation at the trailing edge of the roughened runner blade which provides additional lift (Kuiper 1997).

There are certain findings in the literature which suggest that the surface roughness has an important role in defining the hydrodynamics of the flow through hydraulic turbines. Years of operation alters the surface characteristics of the hydraulic turbines due to many reasons like cavitation erosion, the abrasive action of debris, corrosion, and cracks (Yuan *et al.* 2014). There are a few studies performed on the effects of surface roughness that too are concentrated only on the transposition of model performance to prototype and cavitation erosion (Ida 1990, 1989). Standard; International Electro-Technical Commission standard IEC 60193 provides a guideline about transposition of model results to prototype and set a basis for scaling effects and methodology for taking into account the surface roughness effects. Concerning certain open areas for improvement, International Electro-Technical Commission standard IEC 62097 Edition-2 is a step forward that standardizes for scaling of different losses and surface roughness in hydraulic machines. Wassong *et al.* (2019) worked to disseminate the approaches guided in IEC 62097 Edition-2 about the transposition of model results to prototype. In their work, they have also mentioned the minimum roughness values (based on the specific hydraulic energy) for every component of the prototype along with the suitable roughness measurement techniques suggested in the standard. It was emphasized that surface roughness effects along with Reynolds number (Re) also contribute to frictional losses, and it is very important to take into account while transposition of hydraulic performance. It is also needed to specify minimum roughness (threshold values) to each component of the turbine as excessive smooth surfaces could not contribute to additional efficiency gain. Moreover, there are indications from previous research that small roughness values applied (Ra) on turbine components may decay within a few months of operation. Ahmed *et al.* (1990) carried out a study about cavitation erosion stages and co-related those stages with surface roughness utilizing different surface parameters like average roughness (Ra), RMS value of roughness, skewness and kurtosis. In another work, Zhu *et al.* (2016) studied the erosion behaviour of aluminium alloy AlSi10Mg due to cavitation induced by test rig ASTM G134. Different topographies of the material surface were obtained using grinding, turning, polishing, and laser texturing. It was concluded that the surfaces finished by laser texturing exhibited higher erosion rates. However, surface topography effects on cavitation erosion of the material were found insignificant. Back in 1965, researchers (Numachi, 1967; Numachi *et al.* 1965) worked to see the effects of surface roughness on the cavitation performance of hydrofoils utilized in axial flow turbines and pumps experimentally (Reports 1 and

3). They have concluded that the surface roughness does not affect significantly the cavitation stalling point and violent vibration range though it advances the cavitation inception. It was found that the roughness tends to displace incipient cavitation towards the leading edge of the turbine. Thus, it is realized that the effect of surface roughness on cavitation characteristics of hydraulic turbines is a very intriguing subject.

It is observed from the literature review that there is not enough work done for realizing the surface roughness effects on the cavitating turbulent flow through a hydraulic turbine, and this is the main motivation for the present work. The research in the past were concentrated mainly on analyzing surface roughness effects on the efficiency characteristics, hydraulic losses, and scaling effects during the transposition of model performance to prototype hydraulic turbines. A noticeable literature gap is found in determining surface roughness effects on the performance of reaction hydraulic turbines during cavitating turbulent flow regimes. It is important to study the surface roughness effects on the various hydrodynamic phenomena and the overall performance of the turbine in order to develop a better understanding of these effects, and the present work may provide a further fruitful study on the subject. This work is aimed at a comprehensive numerical analysis of a 3MW capacity low head prototype Francis turbine for obtaining cavitation characteristics and the effects of surface roughness on the hydrodynamics of the cavitating turbulent flow. In the analysis, four different operating regimes; part load of 60%, part load of 80%, full load, and overload of 120% are considered. Flow through the turbine is simulated for smooth and rough boundaries of the turbine flow domain. Different components of the turbine are assigned different sand grain roughness sizes according to IEC 62097 Edition-2 and a study performed by Maruzewski *et al.* (2009). A detailed comparative study of the flow hydrodynamics (hydrodynamic behavior of the flow passing through the flow domain of the turbine) with and without cavitation for smooth and rough turbine passages is carried out. A discussion on the variation of different flow parameters at different operating regimes for smooth and rough turbine boundaries is one of the highlights of the work. All the velocity components such as absolute velocity (C), meridional velocity (C_m), whirl velocity (C_u) and relative velocity (W) are normalized by using the velocity obtained from the rated head (H) in order to give generalized values of these parameters. The obtained results are validated with experimental and previous studies results.

2. METHODOLOGY

The numerical analysis is carried out by following methodology given in the subsequent sections.

2.1 Modelling and Discretization of the Computational Domain

The computational domain consists of a spiral casing, stay ring with 18 stay vanes, distributor with 18 guide vanes, runner with 13 blades and a draft tube. The runner diameter is 1.02m. The geometry of different components is modeled and modified using CREO 5.0 and ICEM CFD with careful incorporation of different level of intricacies to different components by maintaining a balance between feasibility and accuracy. Fig. 1 shows the complete assembly of the turbine.
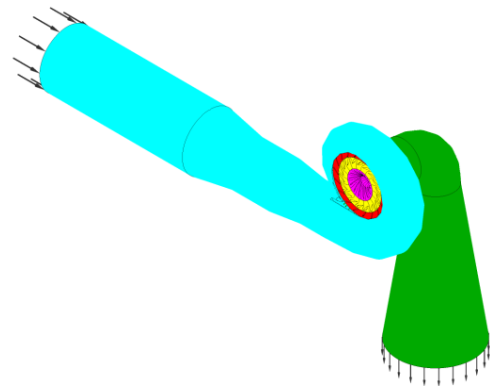

Fig. 1. Computational domains (geometry of the turbine)

Now, the complete flow domain is discretized using a combination of high quality structured and unstructured grids. Components like spiral casing, stay vanes and draft tube are divided into different parts separately for enabling part meshing using ICEM CFD and an unstructured (tetrahedral element type) grid is generated with a controlled size distribution to different parts of an individual component. Runner and distributor domains are discretized through a structured mesh using TURBOGRID by creating flow paths around the passage of their respective blades using ANSYS Design Modeler. The topology of the mesh is set as automatic topology and meshing (ATM) with single round-round symmetric method as the topology generates a high quality structured grid without requiring adjusting control points. This method generates an automatically optimized topology grid using the blade features at different locations of the blade and this is how it manages to create a high quality mesh with less efforts. Fig. 2 shows the grid of the runner domain. In order to check the grid sensitivity of the solution, a grid independency test (GIT) is carried out by utilizing ten different mesh sizes. As runner is the most critical and important element of the turbine because of the flow complexities in the domain, torque produced on the runner is chosen as the varying quantity for the GIT as shown in Fig. 3. The GIT yields an optimum grid size with around 17 million nodes which is then utilized all along for the analysis. Table 1 and Table 2 represent the optimum grid size of different components obtained after GIT and the mesh quality parameters respectively. The values of mesh measures ascertain the high quality of the grid as all the values lie within the permissible range (ANSYS, 2015).
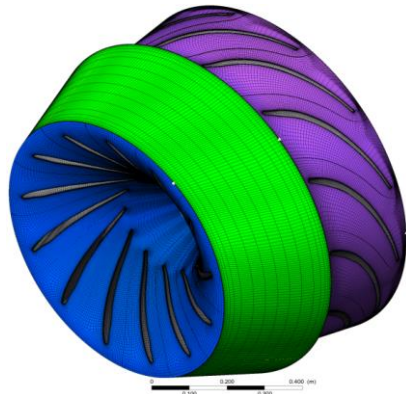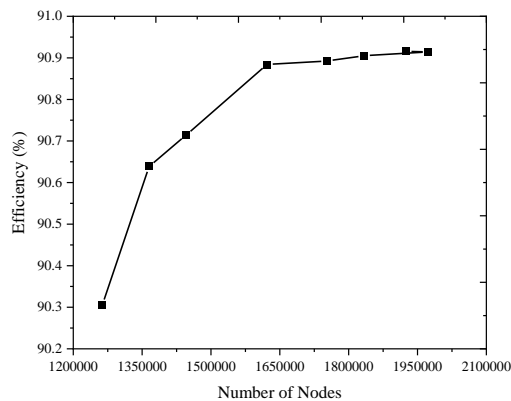
Fig. 2. Grid of the runner flow domain.

Fig. 3. Grid independency test (GIT).

Table 1 Optimum grid size after GIT

Component	Element type	No. of nodes
Spiral casing	Tetrahedron	273955
Stay Ring	Tetrahedron	195772
Distributor	Hexahedron	175997
Runner	Hexahedron	868565
Draft tube	Tetrahedron	201743
Total		1,716,032

Table 2 Generated mesh quality measures

Mesh measure	Value	% Bad
Minimum face angle	26.90^0	0.0
Maximum face angle	152.77^0	0.0
Maximum element volume ratio	3.83	0.0
Minimum volume	$2.33271e\text{-}12 \ m^3$	0.0
Maximum edge length ratio	617.84	0.0
Maximum connectivity number	10	0.0

2.2 Problem Setup and Solution Strategy

The numerical analyses have been carried out for four different cases; without cavitation and with cavitation along with the consideration of smooth and rough boundaries for each. It is noticed that the assigned roughness values to different components are within the limits of threshold values for the specific hydraulic energy range of the turbine as recommended in the standard IEC 62097 Edition-2. The recommended arithmetic average roughness values (R_a) are given in the Table 3. However, RANS based solvers use a single parameter for specifying roughness values to boundaries that is an equivalent sand grain roughness, k_s. There are certain studies carried out in the past to obtain correlations between R_a and k_s based on approaches like surface slope method, moments of heights and that guided in IEC standard (Yuan *et al.* 2014). In the present analysis, the values of k_s have been directly adopted from the work by Maruzewski *et al.* (2009). The roughness values for different components of a real turbine installed at unit 2 of Gordon Merritt Shrum (GMS) generating station (British Columbia Hydro, North-East Vancouver) had been utilized in the work. Moreover, these equivalent sand grain roughness values are within the range specified by Schlichting (1979) based on the Reynolds number (Re). Table 4 shows the equivalent sand grain roughness size considered for different domains in the analysis.

Table 3 Arithmetic average roughness (R_a) values for prototype turbines as recommended in IEC 62097 Edition-2 (Wassong *et al.* 2019)

Roughness applied on	Roughness in µm (for the specific hydraulic energy range 3000-8000 J/kg)
Spiral casing	≥ 3.2
Stay vanes	≥ 1.6
Guide vanes	≥ 0.8
Runner passage	≥ 0.8
Draft tube	≥ 3.2
Rotating part	≥ 1.6
Stationary part	≥ 1.6

Table 4 Equivalent sand grain roughness size (K_s) for different domains (Maruzewski *et al.* 2009; Schlichting 1979)

Domain	Equivalent sand grain roughness size (in µm)
Spiral casing	150
Stay vanes	100
Guide vanes	12.5
Runner	25
Draft tube	50

Different cases are numerically simulated by setting different parameters and solution schemes after importing grids of different components on CFX-Pre. Each component is made as a fluid domain and connected with adjoining components with a fluid-fluid type interface based on GGI method. Conservative interface flux option with no additional interface model is used for modeling mass and momentum through the interface. In order to model interfaces, general connection between the two sides of the interface is considered as it is the most robust

connection type with many frame and pitch change options. Two stationary components are connected with no frame change and pitch change options whereas stationary and rotating components are connected with frozen rotor frame change option along with automatic pitch change. This setting of the interface model allows the solver to obtain steady state solution with assuming pitch change effects between stationary and rotating components. For simulating single phase flow (without cavitation), water is taken as a continuous fluid for the entire flow domain. For defining the domain models, reference pressure is set as 0 Pa along with considering the non buoyant buoyancy model as the buoyancy effects are not significant for single phase water flow. All the domain motions are set as stationary except runner which is a rotating domain with 600 rpm rotational velocity. In the single phase flow, no heat transfer effect is considered, and thus heat transfer model is set as none. However, for capturing turbulence effects shear stress transport model is selected as the turbulence model along with automatic wall function for treating near wall flow.

For simulating the cavitating turbulent flow, water is considered as a continuous fluid and water vapour at 25°C is chosen as a dispersed fluid having mean diameter of 0.05mm. For taking buoyancy effects into account, suitable gravity term is defined to each direction and density difference buoyancy model for both the fluids is chosen along with assigning the reference density as 1000 kg/m^3. For tracing the generated vapour volume fraction in the turbine flow field, homogeneous multiphase model is considered. For cavitating flows, heat transfer effect becomes very important and plays a critical role in predicting the phenomenon. Therefore, total energy heat transfer model is chosen with the inclusion of viscous work term which takes into account the heat generated due to internal fluid friction. For fluid pair modeling, particle model is chosen as an inter-phase transfer model which assumes the dispersed fluid as particles in the continuous fluid. Mass transfer during cavitation is modeled using a model based on Rayleigh Plesset equation (as given in Eq. 5).

For suggesting the solver an initial guess while defining the inlet boundary, vapour and water volume fractions are set as 0 and 1 respectively in order to avoid the over prediction of the cavitation. For realizing the development of cavitation in the turbine space numerically, pressure at the draft tube outlet is varied from 1atm to 0.5atm with a difference of 0.1atm for each load condition. Table 5 shows the boundary conditions implemented for obtaining different cases.

2.3 Governing Equations and Important Expressions

Reynolds averaged Navier-Stokes equations along with two closure equations resulted from the SST k-ω turbulence model have been solved in order to obtain steady state solutions for different set of conditions. Time averaged continuity and momentum equations are given in Eqs. 1 and 2 respectively (ANSYS, 2015).

Table 5 Boundary conditions and guide vane openings for different load operations

Operating regime (% load)	Guide vane opening (^{0})	Mass flow rate at spiral casing inlet (m^3/s)	Static pressure at draft tube outlet (atm)
60	16.2	4.71	0.5-1
80	20.4	5.93	0.5-1
100	24.8	7.2	0.5-1
120	31.1	9.04	0.5-1

$$\frac{\partial \rho}{\partial t} + \frac{\partial}{\partial x_j}\left(\rho U_j\right) = 0 \tag{1}$$

$$\frac{\partial \rho U_i}{\partial t} + \frac{\partial}{\partial X_j}[\rho U_i U_j] = $$
$$-\frac{\partial p}{\partial X_i} + \frac{\partial}{\partial X_j}[\tau_{ij} - \rho\overline{u_i u_j}] + S_M \tag{2}$$

where, τ is the stress tensor which accounts for both normal and shear stress components. $\rho\overline{u_i u_j}$ is the Reynolds stress. For closing the governing equations, the Reynolds stress needs to be modelled. A correlation between the Reynolds stresses and the mean velocity gradients is given by using Boussinesq hypothesis as shown in Eq. 3.

$$-\rho\overline{u_i u_j} = -\rho\frac{2}{3}k\delta_{ij} + \mu_t\left(\frac{\partial\overline{u}_i}{\partial x_j} + \frac{\partial\overline{u}_j}{\partial x_i}\right) \tag{3}$$

where, μ_t is turbulent viscosity which is given as $\mu_t = \rho\dfrac{k}{\omega}$, k is turbulence kinetic energy, δ_{ij} is Kronecker delta, and S_M is the momentum source term.

Total energy equation is also solved along with the other governing equations when the flow involves homogeneous multiphase (water-vapour) flow (ANSYS, 2015). Eq. 4 represents the total energy equation.

$$\frac{\partial \rho h_{tot}}{\partial t} - \frac{\partial P}{\partial t} + \frac{\partial}{\partial X_j}[\rho U_j h_{tot}] = $$
$$\frac{\partial}{\partial X_j}[\lambda\frac{\partial T}{\partial X_j} - \rho\overline{u_j h}] + \frac{\partial}{\partial X_j}[U_i(\tau_{ij} - \rho\overline{u_i u_j})] + S_E \tag{4}$$

where, h_{tot} is the total enthalpy and can be written in the form of static enthalpy as, $h_{tot} = h + 0.5U_iU_i + k$ or $h_{tot} = h + \frac{1}{2}\overline{u}_r^2 - \frac{1}{2}\omega^2 r^2$. Where, k is the turbulent kinetic energy and is given as $k = \frac{1}{2}\overline{u_i^2}$, and $\frac{\partial}{\partial X_j}[U_i(\tau_{ij} - \rho\overline{u_i u_j})]$ is the work due to viscous stresses and is named as viscous work term which accounts for the internal heating due to viscosity of the fluid. It becomes essentially important to employ the viscous work term in the problem setup that involves multiple reference frame (MRF) and total energy equation in order to maintain the consistency in the setup. S_E is the energy source term.

Interphase mass transfer due to cavitation is modeled using model based on Rayleigh Plesset equation which is given as Eq. 5 (ANSYS, 2015).

$$R_B \frac{d^2 R_B}{dt^2} + \frac{3}{2} \left[\frac{dR_B}{dt} \right]^2 + \frac{2\sigma}{\rho_f R_B} = \frac{P_v - P}{\rho_f} \qquad (5)$$

Where, R_B is the bubble radius, P_v is the vapour pressure and is taken as 3170 Pa for the considered working temperature of the fluid, P is the water pressure surrounding the bubble, ρ_f is the water density and σ is coefficient of surface tension on the interface of vapour bubble and water. A generalized equation of mass transfer taking into account the condensation and vapourisation can be given by the Eq. 6 (ANSYS, 2015).

$$\dot{m}_{fg} = F \frac{3 r_{nuc} \left[1 - r_g \right] \rho_g}{R_{nuc}} \sqrt{\frac{2}{3} \left[\frac{|P_v - P|}{\rho_f} \right]} \, \text{sgn} \left[P_v - P \right] \qquad (6)$$

Where, F is a factor which accounts for the different rates of condensation and vapourisation (F_{vap}=50 and F_{cond}=0.01 are the default values used by CFX solver), r_{nuc} is nucleation sites volume fraction and, R_{nuc} is nucleation radius which is taken as 1µm.

Surface roughness induces more turbulence near the wall and that leads to breakdown of viscous sub-layer and increase in wall shear stress. Thus, having a significant impact on hydrodynamics of near wall flow, surface roughness effects must be modeled accurately. Drag augmentation is one of the major surface roughness effects which results in downward shift, ΔB, in the logarithmic velocity profile near the wall (as given in Eq. 7). This downward shift is a function of dimensionless roughness height k_s^+ which is shown in Eq. 8 (ANSYS, 2015). In the RANS based solvers, single parameter which is used to describe roughness is the equivalent sand grain roughness (average roughness height, k_s) (ANSYS, 2015). Equation 9 shows an expression for dimensionless roughness height k_s^+. It is assumed that the roughness induces flow blockage effect which is about 50% of k_s. The fundamental idea behind this is to physically displace the boundary to $k_s/2$ distance in order to account for the roughness effects, and in the governing equations according changes (such as using, $y = \max(y, k_s/2)$) are made. Moreover, turbulent model based on omega equation (like SST k-ω) treats near wall flow by using automatic wall function which utilizes a blending between viscous sub-layer and logarithmic wall region. However, as the roughness height (k_s) increases, the viscous sub-layer gets distorted until it is destroyed in fully rough regimes. This makes the blending between viscous sub-layer and logarithmic region physically not possible. Thus, in order to resolve this difficulty while automatic treatment of rough wall, the walls are physically displaced by 50% height of the roughness element. This shift makes the viscous sub-layer formulation to get affected by small values of k_s^+, and thus the automatic rough wall treatment is carried out during solution. This is how the roughness effects are taken

into account while simulation which will also reflect in macro flow passing through the turbine passage.

$$u^+ = \frac{1}{k} \ln(y^+) + B - \Delta B \qquad (7)$$

$$\Delta B = \frac{1}{k} \ln(1 + 0.3 k_s^+) \qquad (8)$$

$$k_s^+ = \frac{k_s u_\tau}{\nu} \qquad (9)$$

Where, k is Von-Karman constant, B=5.2, u_τ is friction velocity and ν is kinematic viscosity of the fluid.

Thoma cavitation coefficient ($\sigma_{turbine}$) is determined by using the expression given in Eq. 10 (Barlit, 2007).

$$\sigma = \frac{H_{atm} - H_s - H_v}{H} \qquad (10)$$

Where, σ is Thoma cavitation coefficient, H_{atm} is atmospheric pressure head, H_s is suction height (height from tail race level to the centre line of the distributor), H_v is vapour pressure head at the working temperature (here, 25^0 C) and H is the net head across the turbine. The condition for developed cavitation not to occur is $\sigma \geq \sigma_{turbine}$ which ensures that the absolute pressure will not fall below the vapour pressure at the working temperature. The critical value of σ i.e. σ_{cr} beyond which hydraulic efficiency of the turbine drops by 1% is taken as the $\sigma_{turbine}$ (Barlit 2007; Kumar and Saini 2010).

3. RESULTS AND DISCUSSIONS

3.1 Validation

The numerical approach adopted for simulating flow through the Francis turbine is validated with the available experimental and previous work results. The experiments have been carried out on the prototype of a 3MW capacity Francis turbine for three operating conditions. The regime of operation has been varied based on the percentage of load such as 60%, 80% and full load of 100%, and the corresponding discharge values are 4.71m3/s, 5.93m3/s and 7.2m3/s respectively. The experimentally obtained efficiency values for these operating conditions are 85.5%, 90% and 92.6% respectively. Fig. 4 shows the comparison of hydraulic efficiencies obtained from computational and experimental analyses. Maximum difference in efficiency values at corresponding loads is found to be 3% at part load of 60% operation which is well within the acceptable limits. At part load of 60% operation, flow through the runner and draft tube becomes highly unstable due to strong rotor stator interaction (RSI) effects and wobbling vortex rope in the draft tube. In order to capture these flow features, transient analysis needs to be performed which can approximate real flow behaviour more accurately. However, steady flow analysis can provide a reasonable approximation in much less time and CPU cost without resolving time dependent unsteady flow features. After establishing a validity of

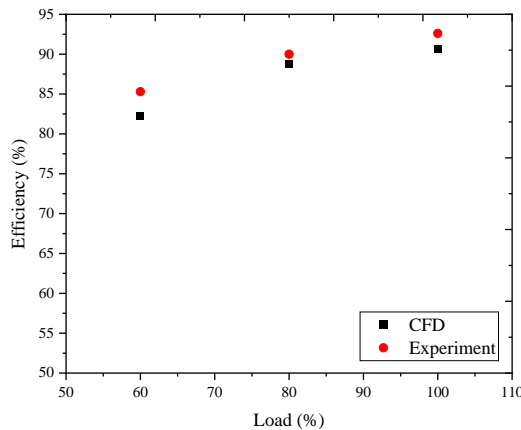computational results, further analyses are carried out.

Fig. 4. Comparison of computational and experimental results.

3.2 Analysis of Flow Parameters for Different Operating Regimes

Analysis of flow hydrodynamics at different operating conditions is carried out with a detailed parametric study by the evaluation of different flow parameters at inlet and outlet of the runner. These parameters include velocity flow angles (β), velocity in stationary frame flow angles (α) and different velocity components (velocity components are normalised from the division of $\sqrt{2gH}$). Table 6 and Table 7 show the values of these flow quantities at different operating regimes for smooth and rough turbine boundaries respectively. A critical inspection of these quantities leads to major findings about flow behaviour in the runner domain at different operating conditions. It is found that the effect of surface roughness on the flow hydrodynamics in the runner is insignificant but, these parameters vary with the operating conditions. At BEP, surface roughness does not have noticeable impact on the flow parameters without and with developed cavitating

regimes of operations. However, for part load of 60% and overload operations, surface roughness effects become significant on these parameters and thus on the hydrodynamics of the flow in the runner. Following are the major findings that can be drawn while analyzing the values of the parameters at different regimes of operations-

(a) At runner inlet, velocity flow angle (β_1) and velocity flow angle at stationary frame (α_1) are found increasing as the turbine boundary changes from smooth to rough for both cavitating and non-cavitating operating conditions. This roughness effect results in decreasing whirl velocity at runner inlet (Cu_1) (except for part load operation of 60% where Cu_1 increases slightly due to roughness). Consequently, angular momentum at the runner inlet decreases. Thus, energy available at the runner inlet also decreases which leads to decrease in hydraulic efficiency and finally overall efficiency of the turbine.

(b) For non-cavitating regimes, velocity flow angle (β_2) and velocity flow angle at stationary frame (α_2) at runner outlet increase because of the surface roughness during part load operations. Consequently, for these regimes, whirl velocity at runner outlet (Cu_2) decreases slightly. However, for full load and overload operations, surface roughness does not have significant effect over the swirl component of velocity at runner outlet. Whereas, for cavitating regimes of operation, roughness plays a critical role in increasing the swirl velocity at runner exit. Velocity triangles at inlet and outlet of the runner give certain idea about the effect of variation of these parameters and help in visualizing the above explanation. Figure 5 shows the inlet and outlet velocity triangles at different operating conditions for smooth and rough turbine surfaces.

3.3 Development of Cavitation in Critical Components of the Turbine

For predicting the cavitation in different domains of the turbine, vapour volume fraction generated in the

Table 6 Different flow parameters at different operating regimes for smooth turbine boundaries

Flow parameters	Operating regime (load of operation)							
	Without cavitation				With cavitation			
	60%	80%	100%	120%	60%	80%	100%	120%
α_1	15.61	19.58	23.85	30.63	15.58	19.55	23.83	30.61
α_2	29.00	34.15	56.04	108.94	30.00	36.51	58.64	103.81
β_1	152.24	147.43	144.01	141.23	152.22	147.40	144.00	141.21
β_2	168.06	165.81	162.53	164.03	143.53	152.37	158.53	160.88
c_{s1}	0.190	0.230	0.268	0.313	0.188	0.226	0.263	0.305
c_{s2}	0.255	0.257	0.280	0.333	0.294	0.311	0.333	0.382
c_{u1}	0.635	0.611	0.570	0.591	0.630	0.598	0.560	0.479
c_{u2}	0.244	0.182	0.095	-0.051	0.226	0.166	0.106	-0.036
w_1	0.394	0.415	0.440	0.479	0.390	0.406	0.432	0.467
w_2	0.640	0.615	0.640	0.726	0.660	0.659	0.640	0.720
c_1	0.666	0.656	0.633	0.588	0.660	0.643	0.623	0.573
c_2	0.354	0.315	0.297	0.341	0.373	0.354	0.350	0.388

Table 7 Different flow parameters at different operating regimes for rough turbine boundaries

Flow parameters	Operating regime (load of operation)							
	Without cavitation				With cavitation			
	60%	80%	100%	120%	60%	80%	100%	120%
α_1	15.67	19.64	23.90	30.65	15.65	19.60	23.88	30.64
α_2	33.93	34.28	55.81	108.40	29.20	36.35	58.37	103.65
β_1	152.27	147.50	144.06	141.24	152.27	147.47	144.02	141.23
β_2	168.49	166.12	162.46	163.93	143.75	152.76	158.55	160.83
c_{s1}	0.191	0.230	0.267	0.312	0.188	0.225	0.262	0.305
c_{s2}	0.272	0.261	0.280	0.333	0.296	0.312	0.331	0.381
c_{u1}	0.638	0.608	0.568	0.586	0.627	0.597	0.557	0.478
c_{u2}	0.241	0.180	0.096	-0.049	0.232	0.168	0.107	-0.035
w_1	0.398	0.415	0.440	0.478	0.391	0.407	0.431	0.466
w_2	0.671	0.621	0.637	0.723	0.661	0.655	0.635	0.717
c_1	0.669	0.654	0.632	0.586	0.658	0.641	0.620	0.572
c_2	0.363	0.319	0.298	0.341	0.377	0.356	0.349	0.387

(b) Inlet velocity triangle   **(a) Outlet velocity triangle**

(I) Part load of 80% operation (non-cavitating regime)

——————— **Smooth Boundaries**
— — — — **Rough Boundaries**

(c) Part load of 80%   **(d) Full Load**   **(e) Overload**

(II) Outlet velocity triangle (cavitating regime)
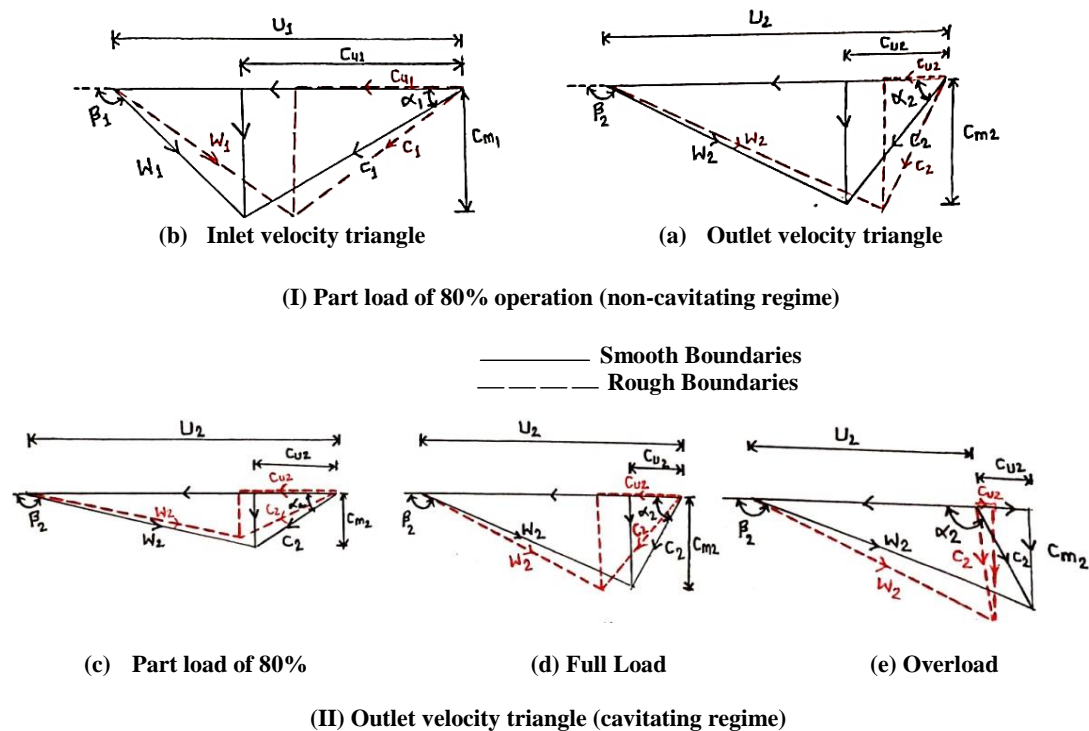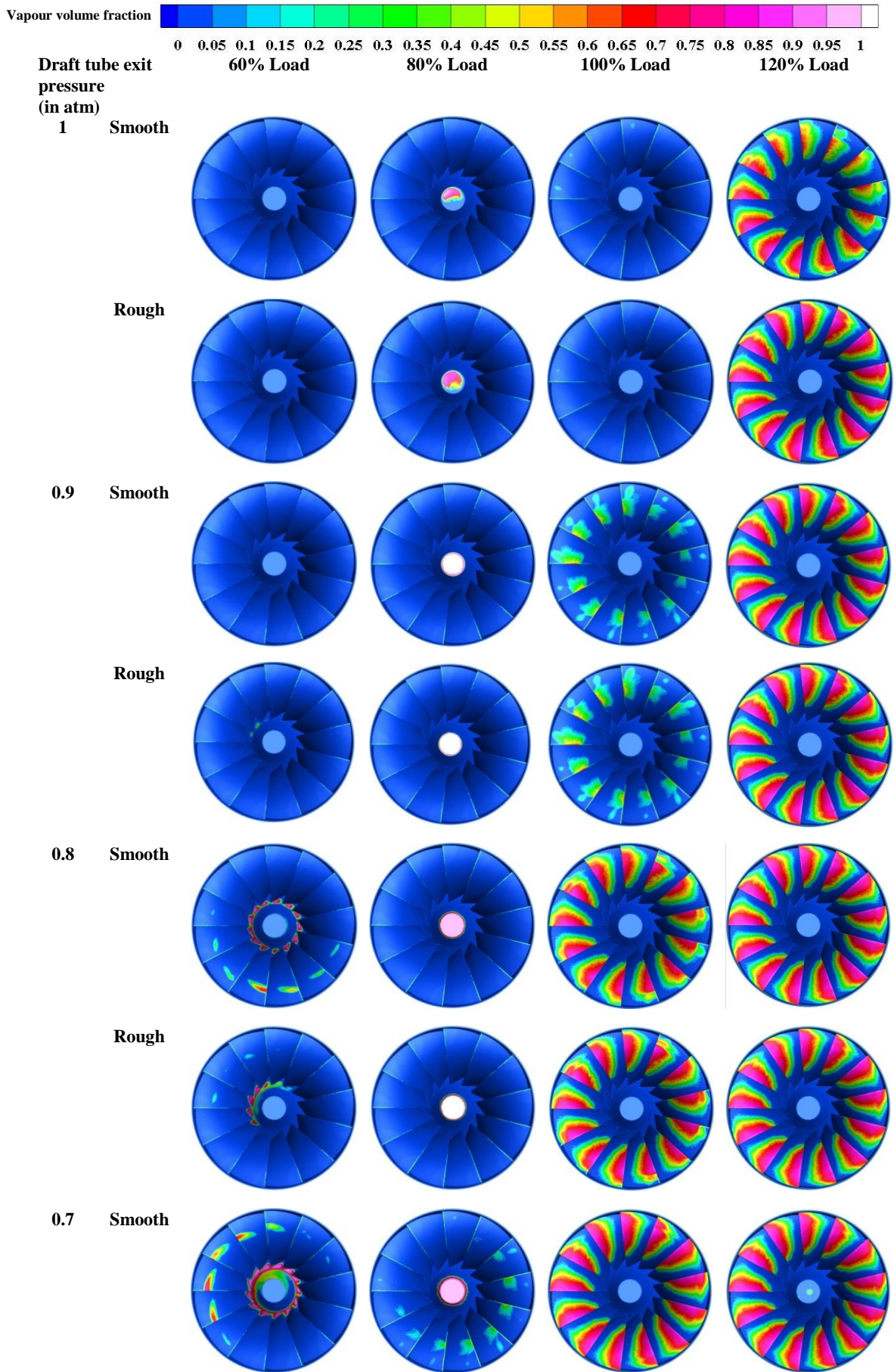
Fig. 5. Inlet and outlet velocity triangles at different operating conditions for smooth and rough turbine surfaces

respective domain is determined. Pressure value at outlet boundary i.e. draft tube outlet is kept on changing from 1 atm to 0.5 atm (as the development is covered within this range for all the operating regimes from part load of 60% to over load) in order to simulate the development stages of cavitation from inception to fully developed stage. Figure 6 shows the development of cavitation in the runner with smooth and rough surfaces. It is seen that the cavitation inception advances with the load for both smooth and rough boundaries because of the increased flow velocities (dynamic vacuum) during higher load operations. Little advancements in

runner core cavitation while part load of 60% operation and profile cavitation during overload operation as a surface roughness effect are observed. The profile cavitation in the overload regime of operation develops a little more towards leading edge of the runner blades. At full load operation which is also the best efficiency point (BEP) of the turbine, surface roughness effect on the cavitation inception is very insignificant. The obtained results are found consistent with the previous studies (Ahmed *et al.*, 1990; Kuiper, 1997; Maruzewski *et al.*, 2009; Numachi, 1967; Yuan *et al.*, 2014; Zhu *et al.*, 2016) wherein the complementing traces can be found.
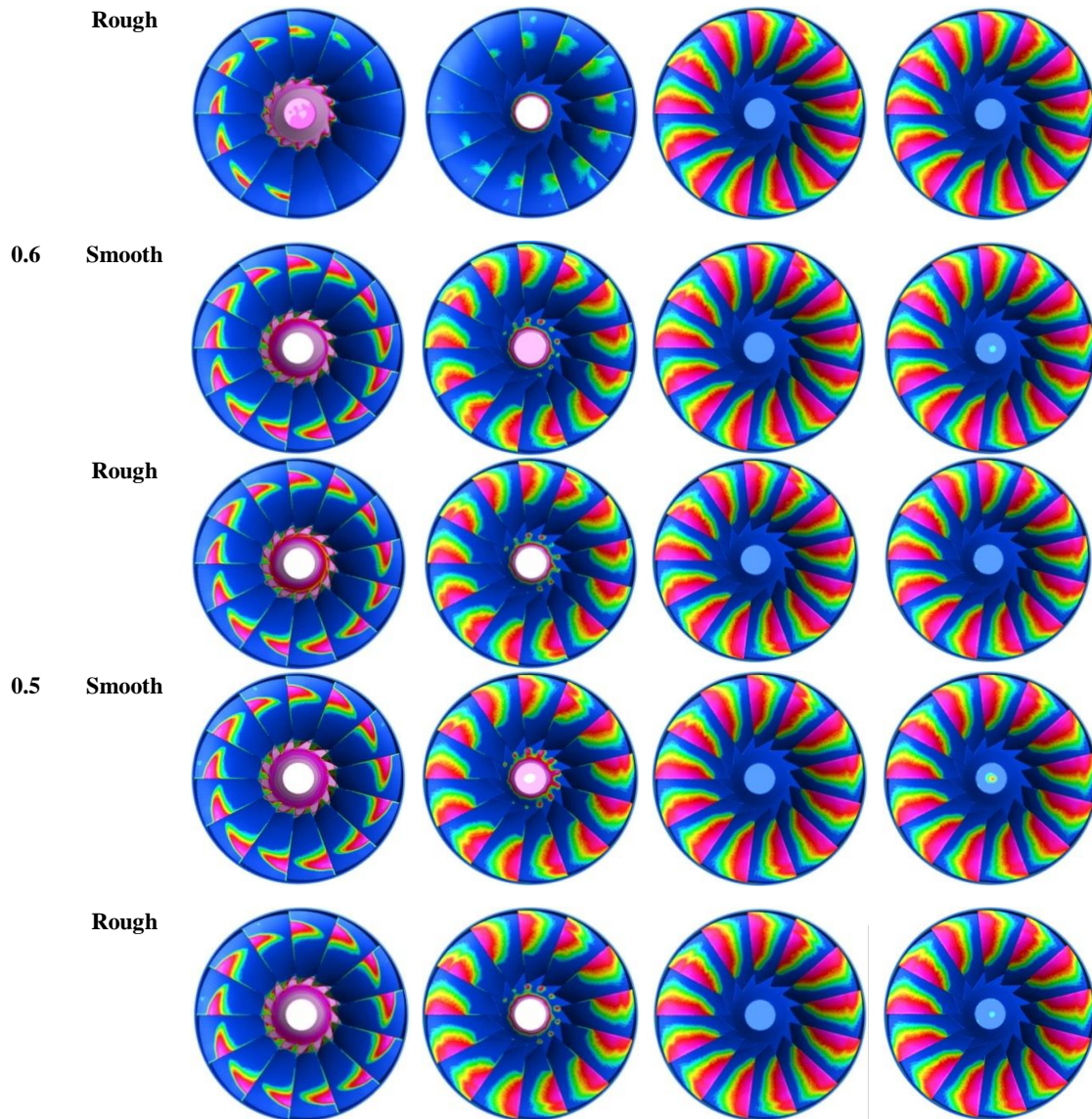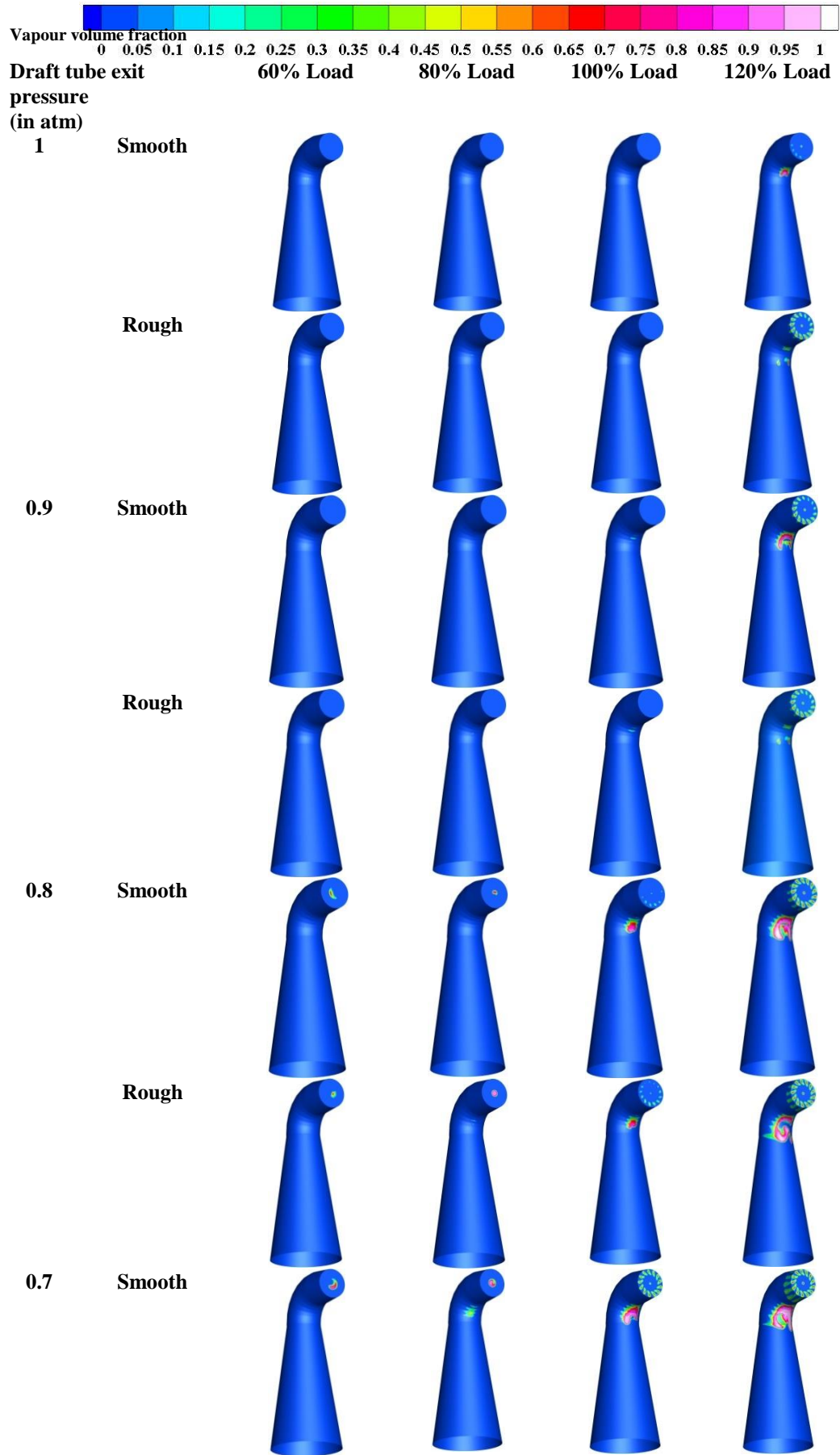
Fig. 6. Development of cavitation in smooth and rough surface runner for different load operations.

If we closely observe the vapour volume fraction generated in the draft tube with smooth and rough boundaries, it can be realized that the roughness has a little impact on the development of cavitation with varying load operations. Figure 7 shows the development of cavitation in the draft tube for different load operations with smooth and rough surfaces. Inner draft tube bend is more prone to cavitation as it realizes sudden change in flow direction along with a local velocity increase which gives rise to localized dynamic vacuum and leads to cavitation inception. It is observed that the developed cavitation in the draft tube is delayed somewhat due to the surface roughness at part load of 60% operation. It is because of the decrement in the local velocity due to eddy dampening effects of surface roughness at 60% load regime. However, for overload operation, roughness promotes eddy formation and results in advancement of cavitation inception. It is observed that the surface roughness assists in dampening eddies in the draft tube during part load operations with and without developed

cavitation. However, during overload operation with developed cavitation, surface roughness promotes the turbulence generation in the draft tube. It is also noticed that surface roughness does not have significant effects on the flow hydrodynamics through the draft tube for full load operation. It can also be concluded that at BEP, surface roughness effects are not significant and hardly alter the flow hydrodynamics for cavitating and non-cavitating regimes.

For part load of 60% operation, blade surface roughness contributes to make pressure gradients even more adverse than that in case of smooth blades for the absence of developed cavitation. However, the blade loading is found almost similar over rough and smooth blades at the regimes with developed cavitation. But, the cavitating flow over rough blades indeed causes lower pressure difference between pressure and suction sides of the blades which in turn results in decreased lift and eventually to less torque generation.
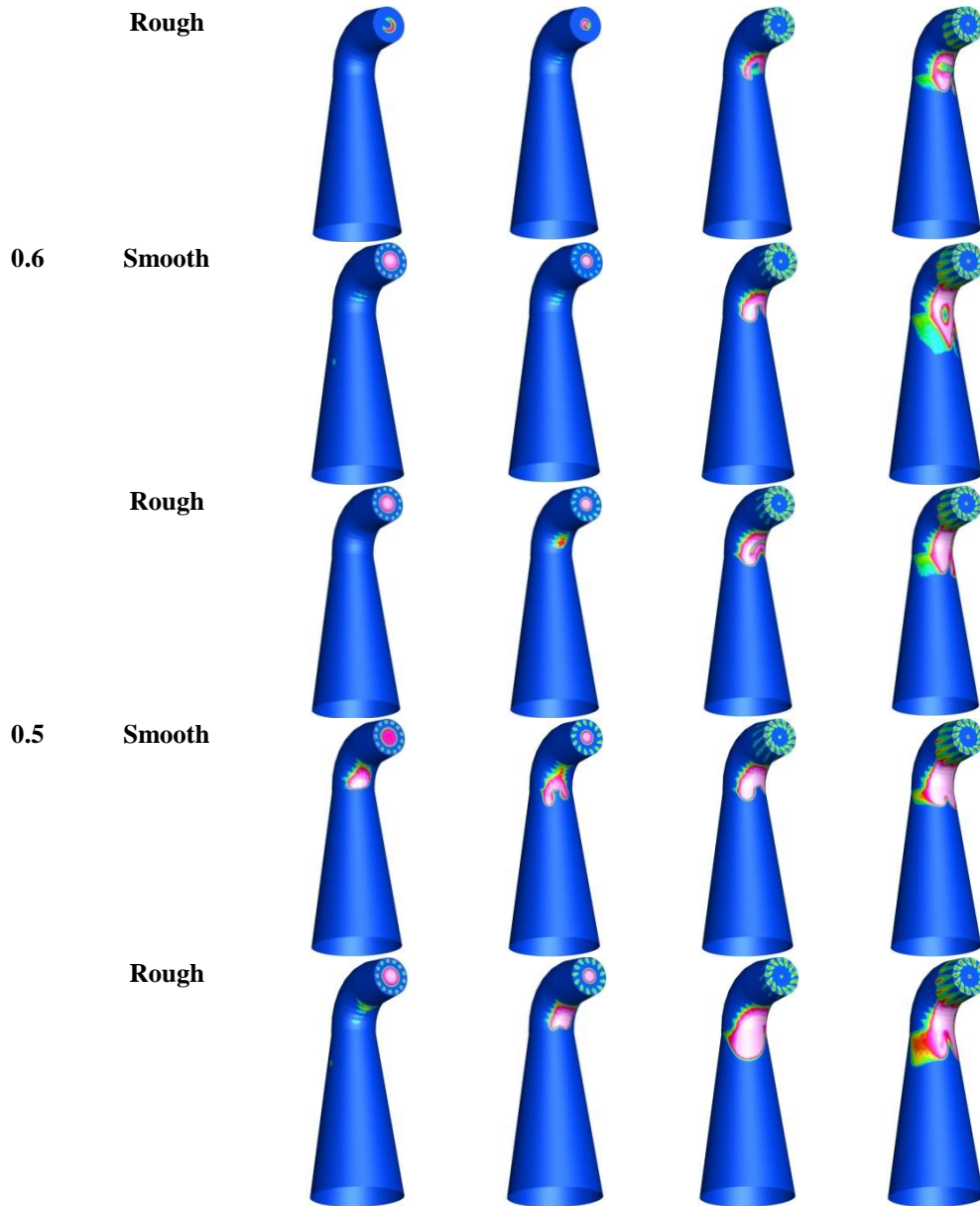
Fig. 7. Development of cavitation in the smooth and rough draft tube for different load operations

Table 8 Torque generated at the runner for different operating conditions

Load (%)	Torque (Nm)			
	Smooth	Rough	Smooth	Rough
	With Cavitation		Without cavitation	
60	28259.2	27989.6	27948.7	28056.5
80	40307.4	40045.9	39933.4	39762.2
100	53002.1	52802.0	53742.3	53444.3
120	73736.6	73529.1	74921.0	74602.2

Table 8 Shows the torque generated on the runner for different operating conditions. The observations from these blade loading curves complement well the study performed by Kuiper (1997).

3.4 Cavitation Characteristics

Cavitation characteristics of the prototype Francis turbine have been derived in order to estimate the critical (turbine) cavitation coefficient for different operating conditions. The value of Thoma cavitation coefficient (σ) beyond which efficiency drops by 1% is taken as critical Thoma cavitation coefficient or turbine cavitation coefficient (Barlit, 2007; Kumar and Saini, 2010). Figure 8 shows the variation of efficiency and unit discharge with sigma for full load operation by considering smooth boundaries. It is observed that discharge passing through the turbine along with the hydraulic efficiency decreases sharply beyond a critical value of sigma, and this drop in efficiency and discharge is steeper in case of rough boundaries. Figure 9 shows the variation of discharge and efficiency with sigma for rough boundaries of the turbine. This characteristic suggests that the roughness makes the operation of
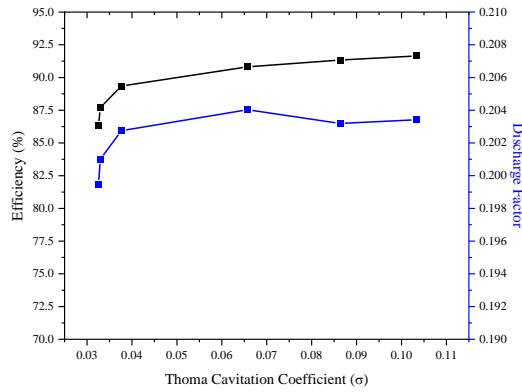
Fig. 8. Variation of efficiency and discharge factor with σ (without roughness) for full load operation.
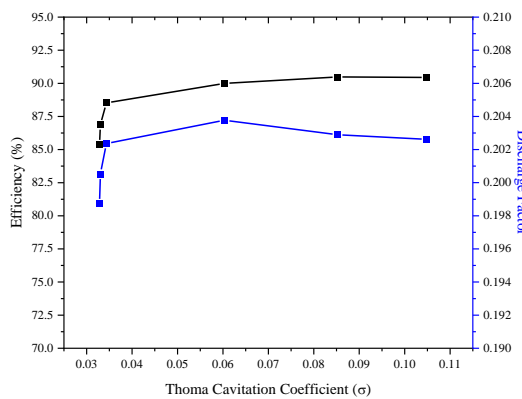

Fig. 9. Variation of efficiency and discharge factor with σ (with roughness) for full load operation.
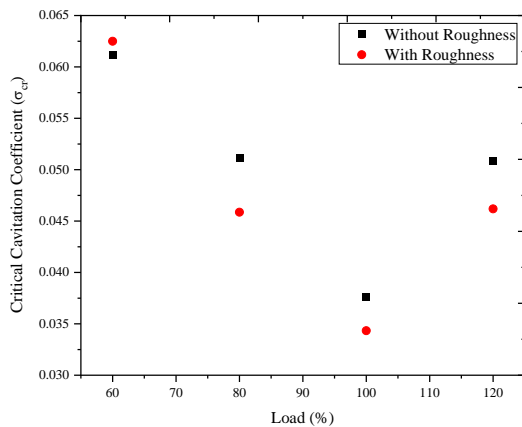

Fig. 10. Comparison of critical cavitation coefficient with and without roughness for different load operations.

the turbine during developed cavitation even more detrimental and may eventually lead to an outage. Figure 10 shows the comparison of critical cavitation coefficients ($\sigma_{turbine}$) obtained for smooth and rough boundaries of the turbine at different load operations. It is seen that the roughness has a significant effect

on the cavitation performance of the turbine. The minimum values of $\sigma_{turbine}$ obtained for the operation at BEP in case of smooth as well as rough turbine boundaries suggest that the turbine functioning near BEP is the least prone to developed cavitation.

It is observed that the roughness may somewhat delay the stage of developed cavitation, but once the stage is reached, it has more detrimental effects on the turbine performance in terms of sharp declined efficiency and increased surface damage.

4. CONCLUSIONS

The adopted computational methodology in the present work is found very effective in order to predict the surface roughness effects on the hydrodynamics of flow through a prototype Francis turbine during cavitating regimes of operations. The obtained results are in fair agreement with the available experimental results and quite consistent with the previous studies. Following are the major conclusions that can be drawn from the present work-

(a) During part load operations, cavitation inception in runner core advances in case of rough boundaries.

(b) For part load of 60% operation, blade surface roughness contributes to make pressure gradients even more adverse than that in case of smooth blades for the absence of developed cavitation.

(c) Surface roughness effect on the flow through the draft tube at BEP is insignificant during developed cavitation and without cavitation operations.

(d) For part load operations, rough boundaries assist to dampen the eddy formation to some extent in the draft tube. This effect leads to less pressure reduction at the bend and leaves the location less prone to the developed cavitation.

(e) During overload operation, surface roughness effects remain negligible in the absence of cavitation but with developed cavitation, these effects become more detrimental to the functioning of the draft tube.

(f) Cavitation characteristic at BEP suggests that the roughness makes the operation of the turbine during developed cavitation even more detrimental and may eventually lead to an outage.

(g) The roughness may result in delayed developed cavitation but once the stage is reached, it deteriorates the turbine performance faster than in case of smooth boundaries.

REFERENCES

Ahmed, S. M., K. Hokkirigawa, R. Oba and Y. Matsudaira (1990). Developing stages of ultrasonically produced cavitation erosion and corresponding surface roughness. *JSME International Journal. Ser. 2, Fluids Engineering, Heat Transfer, Power, Combustion, Thermophysical Properties* 33, 11–16.

ANSYS (2015). ANSYS CFX-solver theory guide, Vol. Release 16.0.

Ayancik, F., E. Acar, K. Celebioglu and S. Aradag (2017). Simulation-based design and optimization of Francis turbine runners by using multiple types of metamodels. *Proceedings of the Institution of Mechanical Engineers, Part C: Journal of Mechanical Engineering Science* 231, 1427–1444.

Barlit, V. V. (2007). *Hydraulic Turbines (Hydraulic Theory, Computations and Experimental Investigations), Vol-1, Vol-2.* Maulana Azad National Institute of Technology Bhopal.

Celebioglu, K., B. Altintas, S. Aradag and Y. Tascioglu (2017). Numerical research of cavitation on Francis turbine runners. *International Journal of Hydrogen Energy* 42, 17771–17781.

Drtina, P. and M.Sallaberger (1999). Hydraulic turbines—basic principles and state-of-the-art computational fluid dynamics applications. *Proceedings of the Institution of Mechanical Engineers, Part C: Journal of Mechanical Engineering Science* 213, 85–102.

Dutta, R., J. Nicolle, A. M. Giroux, U. Piomelli (2016). Evaluation of turbulence models on roughened turbine blades. *IOP Conference Series: Earth and Environmental Science. IOP Publishing*, 62007.

Escaler, X., E. Egusquiza, M. Farhat, F.Avellan and M. Coussirat (2006). Detection of cavitation in hydraulic turbines. *Mechanical Systems and Signal Processing* 20, 983–1007.

Gohil, P. P. and R. P. Saini (2016). Numerical Study of Cavitation in Francis Turbine of a Small Hydro Power Plant. *Journal of Applied Fluid Mechanics* 9, 357-365.

Gohil, P. P. and R. P. Saini (2014). Coalesced effect of cavitation and silt erosion in hydro turbines—a review. *Renewable and Sustainable Energy Reviews* 33, 280–289.

Ida, T. (1990). Analysis of scale effects on performance characteristics of hydraulic turbines: Part 2: Effects of surface roughness, runner seal clearance and Reynolds number on performance and loss distribution coefficients. *Journal of Hydraulic Research* 28, 93–104.

Ida, T. (1989). Analysis of scale effects on performance characteristics of hydraulic turbines: Part 1: Scale formulae of hydraulic performance and loss distribution coefficients in model Francis turbines and pump-turbines. *Journal of Hydraulic Research* 27, 809–831.

Khare, R., D. K. Patel and G. Tiwari (2020). Effect of blade profile on performance of Squirrel Cage Darrius turbine. *AIP Conference Proceedings* 2273, 050029.

Kuiper, G. (1997). Cavitation research and ship propeller design. *Applied Scientific Research* 58, 33–50.

Kumar, J., Y. K. Baghel, G. Tiwari, A. Rawat and V. K. Patel (2020a). Effect of swirl vanes angle on erosion behaviour of AISI 316 pipe bend. *Materials Today Proceedings* 26, 781-786.

Kumar, J., G. Tiwari, A. Rawat and V. K. Patel (2020b). Computational investigation of erosion wear on industrial centrifugal pump handling solid-water flows. *Tribology in Industry* 42, 382-399.

Kumar, P. and R. P. Saini (2010). Study of cavitation in hydro turbines—A review. *Renewable and Sustainable Energy Reviews* 14, 374–383.

Lahdelma, S. and E. K. Juuso (2008). Vibration analysis of cavitation in Kaplan water turbines. *IFAC Proceedings Volumes* 41, 13420–13425.

Laouari, A. and A. Ghenaiet (2016). Simulations of steady cavitating flow in a small Francis turbine. *International Journal of Rotating Machines* 4851454.

Liu, S., L. Zhang, M. Nishi and Y. Wu (2009). Cavitating turbulent flow simulation in a Francis turbine based on mixture model. *Journal of Fluids Engineering* 131.

Luo, X., B. Ji and Y. Tsujimoto (2016). A review of cavitation in hydraulic machinery. *Journal of Hydrodynamics Ser. B* 28, 335–358.

Maruzewski, P., V. Hasmatuchi, H. P. Mombelli, D. Burggraeve, J. Iosfin, P. Finnegan and F. Avellan (2009). Surface roughness impact on Francis turbine performances and prediction of efficiency step up. *International Journal of Fluid Machinery and Systems* 2, 353–362.

Numachi, F. (1967). Effect of Surface Roughness on Cavitation Performance of Hydrofoils—Report 3. *Journal of Basic Engineering* 89, 201-209.

Numachi, F., R. Oba and I. Chida (1965). Effect of surface roughness on cavitation performance of hydrofoils—Report 1. *Journal of Basic Engineering* 87, 495-502.

Schlichting, H. (1979). *Boundary layer theory.* McGraw-Hill New York.

Tiwari, G., S. N. Shukla, V. Prasad and V. K. Patel (2020a). Numerical investigation of hydrodynamics of the cavitating turbulent flow in a low head prototype Francis turbine. *AIP Conference Proceedings* 2273, 050006.

Tiwari, G., J. Kumar, V. Prasad and V. K. Kumar

(2020b). Utility of CFD in the design and performance analysis of hydraulic turbines — A review. *Energy Reports* 6, 2410–2429.

Tiwari, G., J. Kumar, V. Prasad and V. K. Patel (2020c). Derivation of cavitation characteristics of a 3MW prototype Francis turbine through numerical hydrodynamic analysis. *Materials Today Proceedings* 26, 1439-1448.

Tiwari, G., V. Prasad, S. N. Shukla and V. K. Patel (2020d). Hydrodynamic analysis of a low head prototype Francis turbine for establishing an optimum operating regime using CFD. *Journal of Mechanical Engineering and Sciences* 14, 6625-6641.

Tiwari, G., V. Prasad, S. N. Shukla and V. K. Patel (2020e). Derivation of complete performance characteristics of a low head prototype Francis turbine using CFD. *Advances in Mechanical Engineering, Lecture Notes in Mechanical Engineering. Springer, Singapore.* 1581-1591.

Wassong, N. P., J. Iosfin, W. Artner and K. Tezuka (2019). A step forward: IEC 62097-Edition 2- Hydraulic Machines, Radial and Axial–

Methodology for Performance Transposition from Model to Prototype. *IOP Conference Series: Earth and Environmental Science. IOP Publishing,* 22051.

Yuan, J., J. Nicolle, U. Piomelli and A. M. Giroux (2014). Modelling roughness and acceleration effects with application to the flow in a hydraulic turbine. *IOP Conference Series: Earth and Environmental Science. IOP Publishing,* 22016.

Zhang, H. and L. Zhang (2012). Numerical simulation of cavitating turbulent flow in a high head Francis turbine at part load operation with OpenFOAM. *Procedia Engineering* 31, 156–165.

Zhu, Y., J. Zou, W. L. Zhao, X. B. Chen, H. Y. Yang (2016). A study on surface topography in cavitation erosion tests of AlSi10Mg. *Tribology International* 102, 419–428.

Zuo, Z., S. Liu, D. Liu, D. Qin and Y. Wu (2015). Numerical analyses of pressure fluctuations induced by interblade vortices in a model Francis turbine. *Journal of Hydrodynamics* 27, 513–521.